Naphthalene-Based Microporous Polyimides: Adsorption Behavior of CO2 and Toxic Organic Vapors and Their Separation from Other Gases

ARTICLE *in* THE JOURNAL OF PHYSICAL CHEMISTRY C · NOVEMBER 2013

Impact Factor: 4.77 · DOI: 10.1021/jp408502t

THE JOURNAL OF PHYSICAL CHEMISTRY C

Article

pubs.acs.org/JPCC

Naphthalene-Based Microporous Polyimides: Adsorption Behavior of CO_2 and Toxic Organic Vapors and Their Separation from Other Gases

Guiyang Li and Zhonggang Wang*

State Key Laboratory of Fine Chemicals, Department of Polymer Science and Materials, School of Chemical Engineering, Dalian University of Technology, Dalian 116024, China

Supporting Information

ABSTRACT: Naphthalene was selected as a building block to prepare three polyimide networks with different topological structures via one-pot polycondensation from naphthalene-1,4,5,8-tetracarboxylic dianhydride with tetrakis(4-aminophenyl)methane, tris(4-aminophenyl)amine, and 1,3,5-tris(4-aminophenyl)benzene. The resultant polymers have moderately large BET surface areas with narrow pore size distribution at around 6 Å. Interestingly, it is found that they can uptake 90.5 wt % benzene vapor (298 K, 0.8 bar), and the separation factors of benzene over nitrogen, water, and cyclohexane are as high as 759.3, 40.3, and 13.8, respectively. The high adsorption capacity and selectivity of benzene vapor are attributed to the incorporation of large amount of naphthalene groups in the network since naphthalene is highly hydrophobic in nature and has strong π-electron-delocalization effect. On the other hand, the CO_2 uptakes in polymers reach 12.3 wt % (273 K, 1 bar), and the adsorption curves are reversible. Moreover, the separation factors of CO_2/N_2 and CO_2/CH_4 are 88.6 and 12.9, respectively, superior to many other microporous organic polymers. The above experimental results were analyzed and explained with respect to the kinetic diameters, polarity, critical temperature of the vapors and gases, and the stereoconfiguration of net nodes, porous characteristics, and hydrophobic/hydrophilic nature of the pore walls of the microporous polyimides.

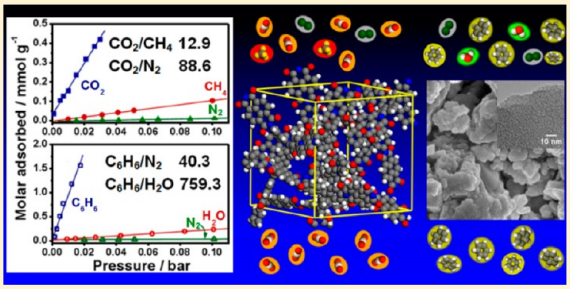

INTRODUCTION

As a new family of functional polymer materials, microporous organic polymers (MOPs) with large surface area and pore size less than 2 nm are being intensely studied,[1−5] and some of them have exhibited promising applications in adsorption and purification of carbon dioxide,[6−10] hydrogen storage,[11−15] heterogeneous catalysis,[16,17] membrane separation,[18−20] optical and low-k materials,[21] etc. Carbon dioxide (CO_2) gas, majorly produced from the burning of fossil fuels and biomass, needs to be removed and recovered because the increasing CO_2 concentration in the atmosphere is regarded as a major reason for global warming. Conventionally, aqueous solutions of amines are employed in power plants to absorb CO_2, but the subsequent recovery of CO_2 and regeneration of amine are rather energy-consuming.[22] In this respect, MOPs have outstanding merits due to their high adsorption capacity of CO_2 at atmosphere pressure and reversible deadsorption process, which makes the regeneration and reuse of the adsorbent very convenient. In addition, the robust covalent bonds linking the building blocks of MOPs confer them with excellent thermal and chemical stability in harsh environments in comparison with other porous solids such as metal−organic frameworks (MOFs).

Toxic volatile organic compounds (VOCs) emitted from petrochemical manufacturing, pharmaceutical industry, solvent production, and the indoor chemical pollutants such as formaldehyde, benzene, and its derivatives released from printing, coating, and household furniture are harmful to human health and environment.[23] In the past years, the removal of VOCs using porous adsorbents like zeolites, activated carbon, activated carbon fibers, and MOFs has been widely studied.[24,25] Despite the significant importance and intense interest in this topic, however, the systematical studies of the adsorption/separation of toxic organic vapors utilizing MOPs are rarely reported up to now. Very recently, some appealing results have revealed the promising potential of MOPs for this purpose. For example, the adsorbed amounts of benzene, hexane, and cyclohexane in PI-ADPM are as high as 99.2, 49.8, and 59.7 wt %, respectively.[26] A porphyrin-based porous polymer also exhibits large uptake capacity of saturated hydrocarbons.[27]

Adsorption capacities of microporous solids for organic vapors and gases are tightly related to the porous properties such as pore size distribution, interconnection of pore channels, surface area, and the physicochemical nature of the pore wall.[28,29] The reported results have shown that the hydrophobic modification of porous zeolites and activated carbons can significantly improve the uptakes of organic vapors and, in

Received: August 25, 2013
Revised: October 24, 2013
Published: October 24, 2013

   dx.doi.org/10.1021/jp408502t | J. Phys. Chem. C 2013, 117, 24428−24437

Scheme 1. Synthesis Routes to the Three Naphthalene-Based Polyimide Networks

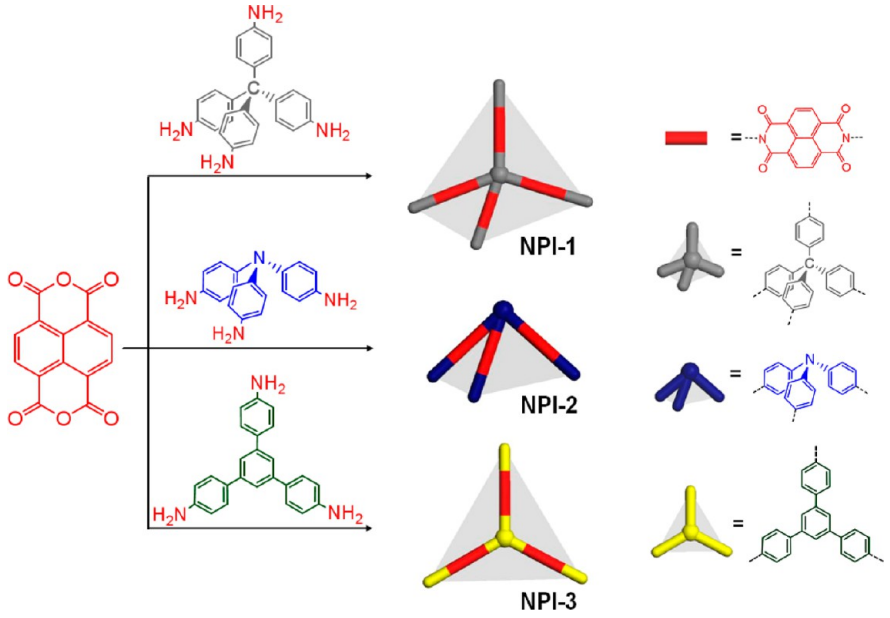

particular, the competitive adsorption with water in humid conditions.[30] As is well-known, naphthalene is a hydrophobic group. Moreover, relative to other building blocks usually used for the preparation of MOPs, naphthalene has a strong π-electron-delocalization effect, which is favorable for the enhancement of affinity toward aromatic vapors. In this regard, the incorporation of naphthalene into MOPs is expected to significantly improve the selective adsorption of toxic benzene and its derivatives over other gases and water vapor.

Previously, naphthalene as a building block has been used to construct microporous polyimides, and the hydrogen storage and CO_2 adsorption at high pressure have been preliminarily studied.[11,31−33] Nevertheless, the adsorption properties of organic vapors and the systematical studies of influence of chemical and porous structures on CO_2 adsorption and separation of CO_2/CH_4 and CO_2/N_2 are still unexplored.

Based on the above consideration, a series of naphthalene-based microporous polyimides with different network topological structures were prepared from naphthalene-1,4,5,8-tetracarboxylic dianhydride with three aromatic multiamine monomers. The focus of the present work is to: (i) Synthesize and well characterize the chemical and porous structures of the three microporous polyimides. (ii) Study the adsorptions of benzene, cyclohexane, and water vapors as well as the separation properties of benzene over nitrogen gas, cyclohexane, and water vapors. Cyclohexane and benzene are chosen as probe molecules because they have similar size and are different only in π-electrons. Thus, we can examine the role of naphthalenes in the microporous network on the selective adsorption of benzene vapor. (iii) Study the influence of pore morphology and stereoconfiguration of building blocks on the adsorption capacities, enthalpies of adsorption, virial coefficients of CO_2, and the separation properties of CO_2/N_2 and CO_2/CH_4 gas pairs in the microporous polyimides.

EXPERIMENTAL SECTION

Materials. Tetraphenylmethane, tris(4-nitrophenyl)amine, 4-nitroacetophenone, and naphthalene-1,4,5,8-tetracarboxylic dianhydride (NTDA) were purchased from J&K Chemical Co., Ltd. NTDA was purified by sublimation prior to use. *m*-Cresol, isoquinoline, and other reagents were purchased from Shanghai Chemical Reagent Co. *m*-Cresol was purified by distillation under reduced pressure and dehydrated with 4A molecular sieves. Isoquinoline, tetrahydrofuran (THF), *N*,*N*-dimethylformamide (DMF), methanol, and other reagents were reagent grade and used as received. Tetrakis(4-aminophenyl)-methane (TAPM), tris(4-aminophenyl)amine (TAPA), and 1,3,5-tris(4-aminophenyl)benzene (TAPB) were prepared according to the procedures described in the literature.[34,35]

Preparation of Polyimide Networks. The polymerization of NPI-1 is carried out in a dry Schlenk flask equipped with a stirrer and a condenser in an ice bath. Under argon flow, TAPM (0.40 g, 1.38 mmol), NTDA (0.56 g, 2.07 mmol), and 10 mL of *m*-cresol were added and stirred for 2 h. After slowly heating to room temperature, a catalytic amount of isoquinoline was added. Then the temperature was raised in the heating schedule: 30 °C for 8 h, 80 °C for 4 h, 160 °C for 4 h, 200 °C for 10 h, and 220 °C for 4 h. Finally, the system was cooled down, and the solid was isolated and washed successively with DMF, methanol, and THF. The resultant product was extracted with THF in a Soxhlet apparatus for 24 h and dried at 120 °C under vacuum to constant weight. A quantitative yield was achieved.

NPI-2 and NPI-3 were prepared in a similar procedure to NPI-1 except that the multiamine monomers used were TAPA and TAPB instead of TAPM, respectively.

Instrumention. Fourier transform infrared spectra (FTIR) of synthesized products were recorded using a Nicolet 20XB FT-IR spectrophotometer in the 400−4000 cm^{-1} range. Samples were prepared by dispersing the complexes in KBr to form disks. ^1H NMR spectra were recorded on a 400 MHz Varian INOVA NMR spectrometer, using tetramethylsilane as an internal standard. Solid-state ^{13}C CP/MAS (cross-polarization with magic angle spinning) spectra were measured on a Varian Infinity-Plus 400 spectrometer at 100.61 MHz at an MAS rate of 10.0 kHz using zirconia rotors 4 mm in diameter using a contact time of 4.0 ms and a relaxation delay of 2.0 s. Elemental analyses were determined with an Elementar Vario

dx.doi.org/10.1021/jp408502t | J. Phys. Chem. C 2013, 117, 24428−24437

EL III elemental analyzer. Wide-angle X-ray diffractions (WAXD) from 5° to 60° were performed on Rigku D/max-2400 X-ray diffractometer (40 kV, 200 mA) with a copper target at a scanning rate of 2° min^{-1}. Field-emission scanning electron microscopy (FE-SEM) experiments were carried on a Nova NanoSEM 450. Before measurements, the samples were sputter-coated with chromium film to facilitate conduction. Transmission electron microscopy (TEM) images were obtained on a Hitachi HT-7700 operated at 100 kV. Thermogravimetric analysis curves were recorded on a NETZSCH TG 209 thermal analyzer by heating the samples (ca. 8 mg) up to 800 °C at the rate of 10 °C min^{-1} under both nitrogen and air atmospheres. Adsorption and desorption measurements for all the gases and vapors were conducted on an Autosorb iQ (Quantachrome) analyzer. Prior to measurements, the samples were degassed at 150 °C under high vacuum overnight. Adsorption and desorption isotherms of nitrogen were measured at 77 K. The surface areas were calculated according to the Brunauer–Emmett–Teller (BET) model in the relative pressure (P/P_0) range from 0.12 to 0.20 for NPI-1, NPI-2, and NPI-3. CO_2 and CH_4 adsorption isotherms were measured at 273 and 298 K up to 1.0 bar. The adsorptions of benzene, cyclohexane, and water vapors were measured with the pressure up to the saturated vapor pressure at 298 K. N_2 adsorption isotherms at 273 and 298 K were measured in order to evaluate the adsorption selectivities of CO_2/N_2 and benzene/N_2.

RESULTS AND DISCUSSION

Synthesis and Characterization of Naphthalene-Based Polyimide Networks. Three naphthalene-based microporous polyimides, NPI-1, NPI-2, and NPI-3, were prepared via one-pot polycondensation from TAPM, TAPA, and TAPB with NTDA, respectively, using *m*-cresol as reaction medium and isoquinoline as a catalyst (Scheme 1). The system temperature was raised slowly in several steps so that the polymerization could proceed smoothly to achieve homogeneous cross-linking network. In thus-synthesized NPI-1, NPI-2, and NPI-3 networks, the linking strut is a naphthalimide unit, whereas the net nodes are tetraphenylmethane, triphenylamine, and 1,3,5-triphenylbenzene, respectively. After purification by Soxhlet apparatus, brown solid powders were obtained. All the products could not dissolve in any common solvents, indicative of the hyper-cross-linked structures.

FTIR spectra of the initial monomers are presented in Figure S1 (Supporting Information). For the three multiamine monomers (TAPM, TAPA, and TAPB), the absorption at 1621 cm^{-1} is assigned to the deformation vibration of the N–H bond. The characteristic band for the carbonyl of a six-membered anhydride group of NTDA appears at 1778 cm^{-1}. After polymerization, the three naphthalene-based polyimides display two strong absorptions at 1720 and 1670 cm^{-1} (Figure 1), which resulted from the typical symmetric and asymmetric vibrations of C=O group belonging to the formed six-membered imide ring. The band at 1345 cm^{-1} is assigned to the C–N–C stretching vibration. The FTIR data indicate that NTDA has been successfully polymerized with multiamine monomers to generate naphthalene-based polyimides. Additionally, it is noted that, for the three polymers, a weak absorption at 1781 cm^{-1} can be detected, implying that the condensation polymerizations between anhydride and amine group are not very complete. In solid-state ^{13}C CP/MAS NMR spectra (Figure 2), the characteristic carbon resonance in imide

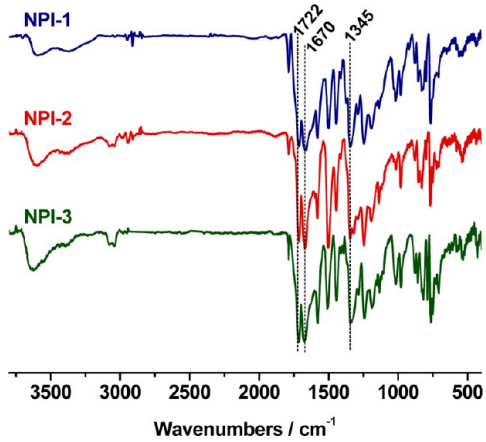

Figure 1. FTIR spectra of the three naphthalene-based polyimide networks.

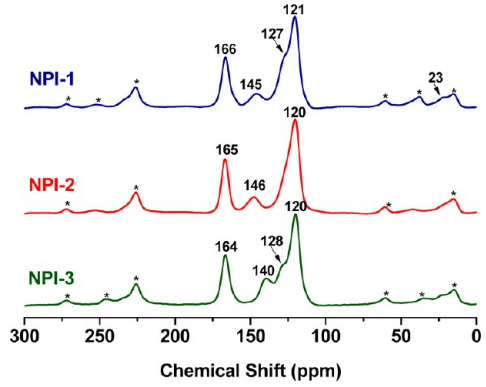

Figure 2. Solid-state ^{13}C CP/MAS NMR spectra for NPI-1, NPI-2, and NPI-3. Asterisks indicate peaks arising from spinning side bands.

ring appears at around 165 ppm. The quaternary carbon in NPI-1 locates at 23 ppm, the N-substituted phenyl carbon is at about 145 ppm, and the overlapping signals from 121 to 137 ppm belong to the other aromatic carbons in backbone. Elemental analyses show that the calculated elemental composition in each case is roughly consistent with the measured values (Table S1, Supporting Information). The slight deviation of hydrogen and nitrogen contents is caused by the absorbed moisture and CO_2 in air.

To investigate the thermal stabilities of the porous polyimide networks, thermogravimetric (TGA) measurements under both nitrogen and air atmospheres were conducted in the range from 25 to 800 °C. As shown in Figure 3, the oxidative environment seems to have no obvious effects on the initial thermal degradation temperatures. All the samples exhibit the temperatures with 2.5% weight loss over 480 °C, indicative of excellent heat resistance. Under a nitrogen atmosphere, the char yields at 800 °C are 50.0, 46.7, and 64.7 wt % for NPI-1, NPI-2, and NPI-3, respectively. However, the air atmosphere results in the samples apparently decreased char yields.

The WAXD patterns (Figure S2) display that all the polyimide networks are amorphous in nature. Their surface morphologies were examined by field-emission scanning electron microscopy (Figure 4a–c). Similar to other microporous polymers,[36] the samples are homogeneous, composed of loose agglomerates of tiny particles with rough surface and irregular shape. Besides, uniform microporous channels can be

dx.doi.org/10.1021/jp408502t | J. Phys. Chem. C 2013, 117, 24428–24437

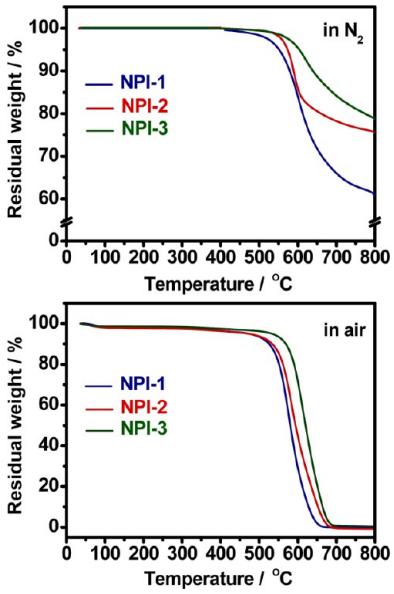

Figure 3. TGA curves of NPI-1 (blue), NPI-2 (red), and NPI-3 (green) under nitrogen and air atmospheres.

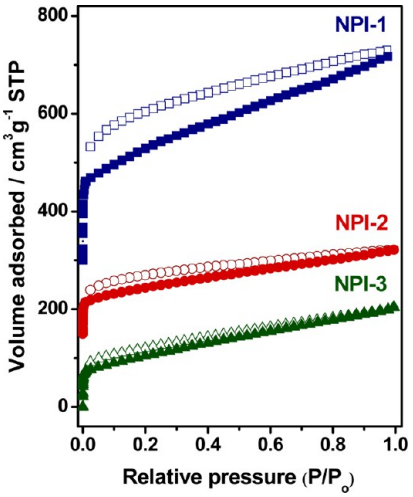

Figure 5. Adsorption (filled) and desorption (empty) isotherms of N_2 in NPI-1 (+300), NPI-2 (+150), and NPI-3.

observed by means of high-resolution transmittance electron microscopy (Figure 4a′−c′).

Porous Structure of Naphthalene-Based Polyimide Networks. The surface areas and porosity parameters of the polyimide networks were studied by physical sorption of nitrogen at 77 K (Figure 5). The isotherms exhibit rapid nitrogen uptake at the very low relative pressure, indicating the existence of large amount of permanent micropores. The adsorption−desorption hysteresis can be attributed to the deformation of the network structure probably caused by the swelling effect of liquid nitrogen.[37] In our cases, the naphthalene-based microporous polymers are amorphous in nature. To generate porous structure, the net node should be rigid and the stereoconfiguration should efficiently prevent the segments of networks from packing. The results in Table 1 reveal that the three-dimensional tetrahedral shape for the rigid TAPM is favorable for this purpose. Among the three samples, NPI-1 possesses the highest BET surface area of 721 $m^2\ g^{-1}$, Langmuir surface area of 1081 $m^2\ g^{-1}$, and total pore volume of 0.51 $cm^3\ g^{-1}$. In contrast, NPI-2 and NPI-3 have the topological structures similar to two-dimensional planar network. Subsequently, BET surface areas of NPI-2 and NPI-3 are only 291 and 373 $m^2\ g^{-1}$, respectively.

The pore sizes and distributions for NPI-1, NPI-2, and NPI-3 are calculated by the nonlocal density functional theory (NLDFT) from the sorption curves of nitrogen at 77 K. As shown in Figure 6, except for the small amount of pores in NPI-3 at 2.07 nm, the major pores in the three samples locate

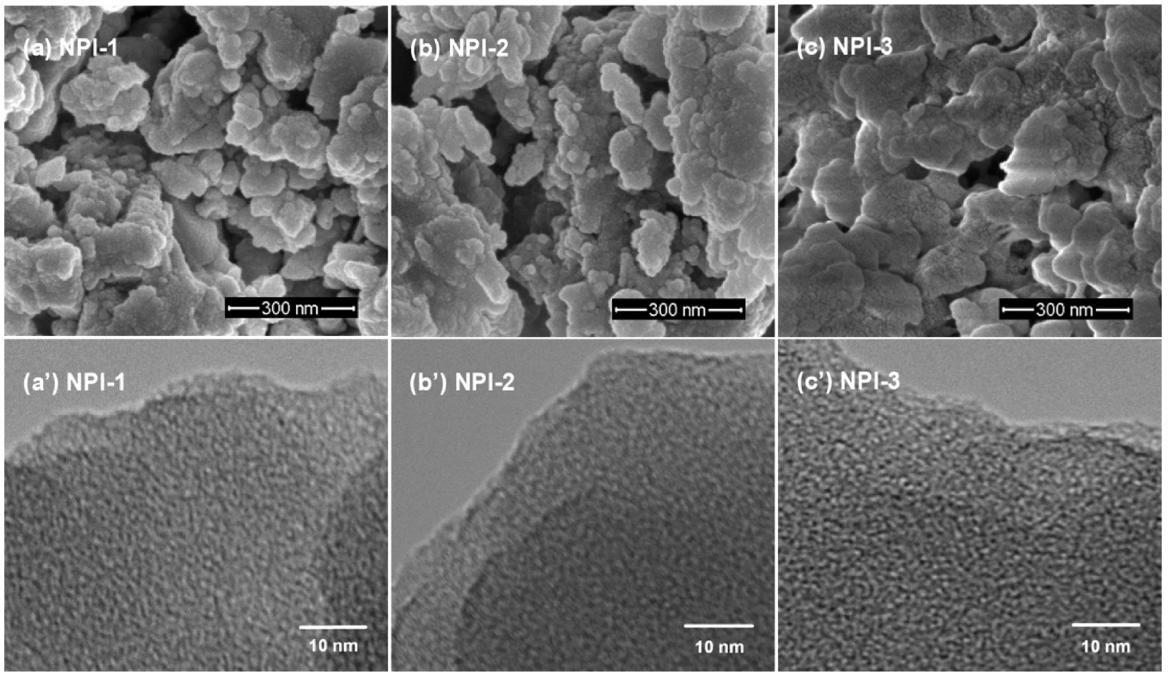

Figure 4. FE-SEM images of NPI-1 (a), NPI-2 (b), and NPI-3 (c). HR-TEM images of NPI-1 (a′), NPI-2 (b′), and NPI-3 (c′).

dx.doi.org/10.1021/jp408502t | J. Phys. Chem. C 2013, 117, 24428−24437

Table 1. Pore Parameters of the Naphthalene-Based Microporous Polyimides

samples	S_{BET} (m^2 g^{-1})	$S_{Langmuir}$ (m^2 g^{-1})	S_{micro} (m^2 g^{-1})	V_{total} (cm^3 g^{-1})	V_{micro} (cm^3 g^{-1})	pore size (nm)
NPI-1	721	1081	360	0.51	0.15	0.60
NPI-2	291	438	151	0.20	0.07	0.59
NPI-3	373	567	157	0.29	0.08	0.57, 2.07

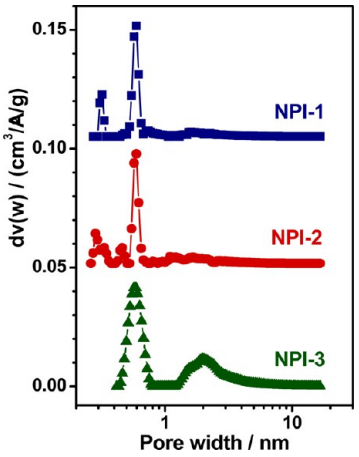

Figure 6. Pore size distribution curves for NPI-1 (+0.10), NPI-2 (+0.05), and NPI-3.

at around 0.6 nm, indicating that the resultant naphthalene-based polyimides belong to microporous polymers.

Selective Adsorption of Organic Vapors in the Porous Polyimides. In this study, one of our main motivations is to investigate the effect of naphthalene groups in the network on the selective adsorption of benzene vapor over nitrogen, cyclohexane, and water vapors. The adsorption isotherms of vapors measured at 298 K are presented in Figure 7. In contrast

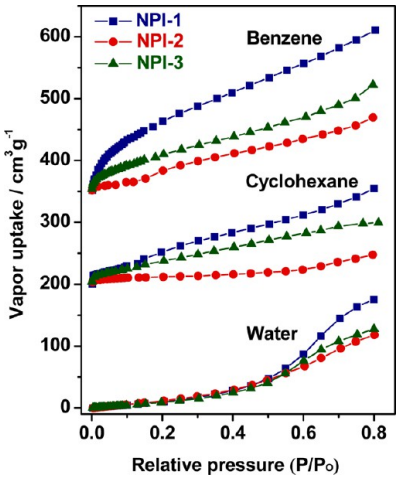

Figure 7. Organic and water vapor adsorption isotherms as a function of the relative pressure at 298 K for three polyimide networks (benzene +350, cyclohexane +200, water).

to cyclohexane and water, for NPI-1 and NPI-3, the benzene vapor uptakes give a rapid rise at the low relative pressure (P/P_0 < 0.1), indicating that the network skeleton composed of naphthyl and phenyl groups has a strong affinity toward benzene molecules. For NPI-2, there is also a small rise at the initial stage, but the adsorption becomes flat in the P/P_0 range of 0.1−0.2 and then grows again. This can be attributed to the reason that, among the three samples, NPI-2 has a smallest surface area, and the saturation adsorption on the pore wall is easily reached. Only at the higher pressure, the pores in the network start to accommodate more benzene molecules. The data in Table 2 show that, at P/P_0 = 0.8, the sorption capacity

Table 2. Uptake of Benzene Vapor and Its Selectivity over Cyclohexane, Nitrogen, and Water at 298 K in the Microporous Polyimides

	vapor uptake[a] (wt %)			benzene selectivity[b] at 298 K		
sample	C_6H_6	*c*-C_6H_{12}	H_2O	C_6H_6/*c*-C_6H_{12}	C_6H_6/N_2	C_6H_6/H_2O
NPI-1	90.5	58.1	14.1	13.8	759.3	40.3
NPI-2	41.5	17.9	9.5	20.7	194.8	10.6
NPI-3	59.9	37.4	10.2	4.4	136.8	12.4

[a]Uptakes for C_6H_6 (benzene vapor), *c*-C_6H_{12} (cyclohexane vapor), and H_2O (water vapor) were determined at P/P_0 = 0.8 and 298 K. [b]C_6H_6/*c*-C_6H_{12}, C_6H_6/N_2, and C_6H_6/H_2O selectivities were calculated from initial slopes of pure-component sorption isotherms.

of benzene is 90.5 wt % in NPI-1, much higher than that in carbon material F42C (39.5 wt %),[38] metal azolate framework MAF-2 (20.6 wt %),[39] and microporous cyanate resin (47.8−58.5 wt %).[40,41] In comparison with aromatic benzene vapor, the aliphatic cyclohexane without π-electrons exhibit apparently lower uptake, demonstrating that the strong $\pi-\pi$ interaction between naphthalene-based polymer skeleton and benzene molecule plays a significant role on the adsorption capacity. In addition, the isotherms for water vapor are typical type III sorption, and its uptakes in NPI-1 is only 14.1 wt %, which is much lower than other porous polymers, such as EOFs,[42] indicative of the hydrophobic nature of the naphthalene-based polyimide networks.

As the adsorption capacity at the very low pressure region can reflect the affinity between the pore wall and the adsorbate, the ratio of initial adsorption slopes of two adsorbates calculated from the adsorption isotherms has been frequently used as their separation factors.[43,44] Therefore, at 298 K, the adsorbed amounts of benzene, cyclohexane, water, and N_2 as a function of pressure in the range from 0 to 0.2 bar are plotted (Figure 8). The separation factors of benzene/cyclohexane, benzene/N_2, and benzene/H_2O are listed in Table 2.

As shown in Table 2, the pore walls of the three polyimides are preferentially adsorbed by benzene rather than cyclohexane. The separation factors of benzene/cyclohexane for NPI-1 and NPI-2 are 13.8 and 20.7, respectively. Considering that benzene and cyclohexane have similar molecular size, the significantly higher adsorption capacities of benzene can be attributed to the strong affinity of benzene molecules toward the abundant naphthyl or phenyl groups in NPIs by virtue of $\pi-\pi$ interaction. Compared to NPI-1 and NPI-2, the relatively lower separation factor of NPI-3 may be caused by the presence of mesopores in the NPI-3 network.

Interestingly, by comparing the initial slope of benzene with that of N_2 and H_2O, it is observed that, for NPI-1, besides the

dx.doi.org/10.1021/jp408502t | J. Phys. Chem. C 2013, 117, 24428−24437

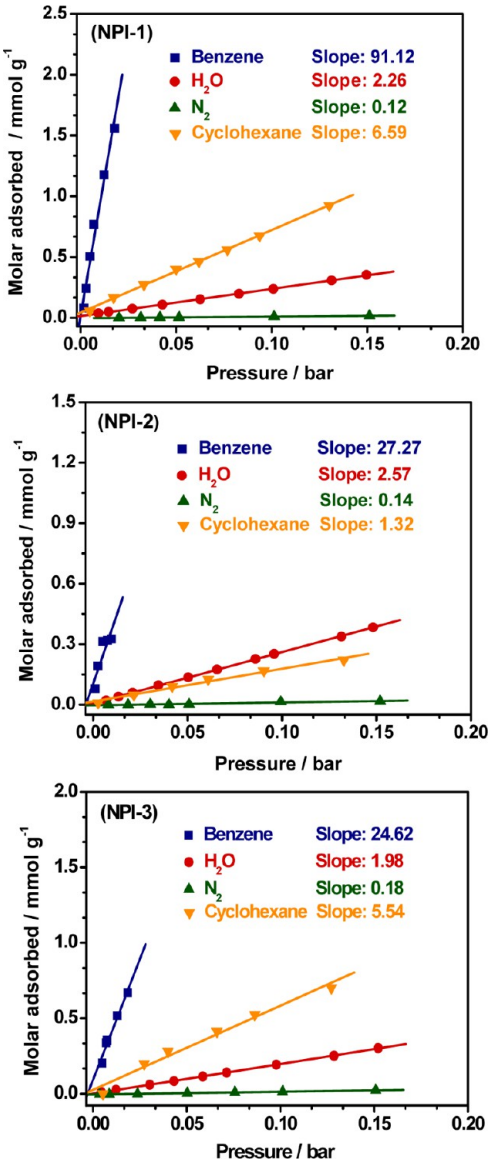

Figure 8. Adsorption selectivity of benzene over H_2O and N_2 for NPIs calculated from initial slope of benzene (blue), cyclohexane (orange), H_2O (red), and N_2 (green) isotherms collected at 298 K.

considerably higher adsorption capacity of benzene (90.5 wt %, 298 K), its separation factor of benzene over N_2 is as high as 759.3. Moreover, the hydrophobic polyimide skeleton gives rise to high benzene/H_2O selectivity of 40.3. The excellent adsorption/separation properties of benzene/N_2 and benzene/H_2O are especially important for the removal of toxic benzene in air and water-cleaning applications.

CO_2 Adsorption/Separation in the Microporous Polyimides. The sorption isotherms of CO_2 at 273 and 298 K are presented in Figure 9a–c. It is found that the CO_2 uptakes appear a rapid rise at the initial stage and have not reached saturation in the experimental range, implying that CO_2 molecule has favorable interaction with the polymer skeleton, and much high storage capacity can be expected at the increased pressure. Moreover, the adsorption–desorption curves of CO_2 are roughly reversible. Thus, after adsorption, the equivalent amount of CO_2 from their cavity can be released while reducing the pressure, which characteristic is quite desirable for the practical operation in CO_2 capture and regeneration of porous adsorbent. The CO_2 adsorption data in Table 3 show that, among the three microporous polyimides,

Table 3. CO_2 Uptake and Its Selectivity over N_2 and CH_4 at 273 and 298 K in the Microporous Polyimides

	CO_2 uptake[a] (wt %)		CO_2 selectivity[b]			
sample	273 K	298 K	CO_2/N_2 at 273 K	CO_2/N_2 at 298 K	CO_2/CH_4 at 273 K	CO_2/CH_4 at 298 K
NPI-1	12.3	7.9	88.6	45.2	12.9	8.7
NPI-2	7.3	4.8	33.6	18.9	12.3	6.4
NPI-3	8.2	5.3	41.3	15.7	11.1	4.1

[a]Uptakes for CO_2 were determined at 273 K, 1 bar and 298 K, 1 bar. [b]CO_2/N_2 and CO_2/CH_4 selectivities were calculated from initial slopes of pure-component sorption isotherms.

NPI-1 exhibits the highest CO_2 uptake of 12.3 wt % at 1 bar and 273 K, which are comparable to or higher than many other porous polymers even if having larger surface area, such as COF-103 (7.6 wt %, 3530 $m^2\ g^{-1}$),[45] CMP-0 (9.2 wt %, 1018 $m^2\ g^{-1}$),[46] and PAF-1 (9.1 wt %, 5640 $m^2\ g^{-1}$)[47]

The isosteric enthalpies of adsorption (Q_{st}) of CO_2 were calculated based on the Clausius–Clapeyron equation:[48]

$$\ln p = \frac{Q_{st}}{RT} + C \quad (1)$$

where P, T, R, and C are the pressure, temperature at the equilibrium state, the gas constant, and equation constant, respectively.

The dependencies of Q_{st} values on the adsorbed amount are shown in Figure 10a. For each sample, the Q_{st} values apparently decrease with the adsorbed amount, meaning that the interaction between CO_2 and pore wall is stronger than that between CO_2 molecules. Noteworthy, the three polymers have the similar chemical structure, but their Q_{st} values are different.

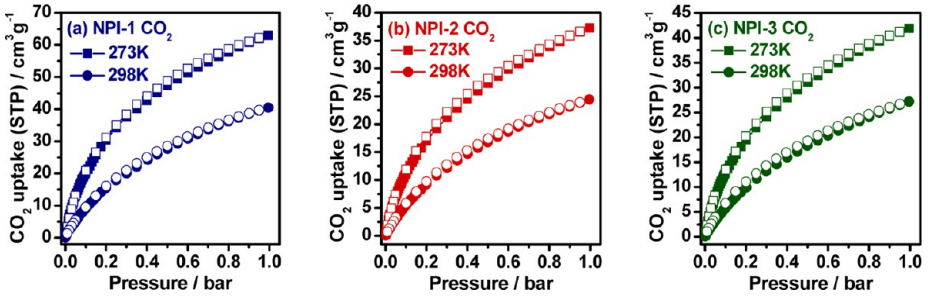

Figure 9. CO_2 Adsorption (filled) and desorption (empty) isotherms (a–c) at 273 and 298 K.

dx.doi.org/10.1021/jp408502t | J. Phys. Chem. C 2013, 117, 24428–24437

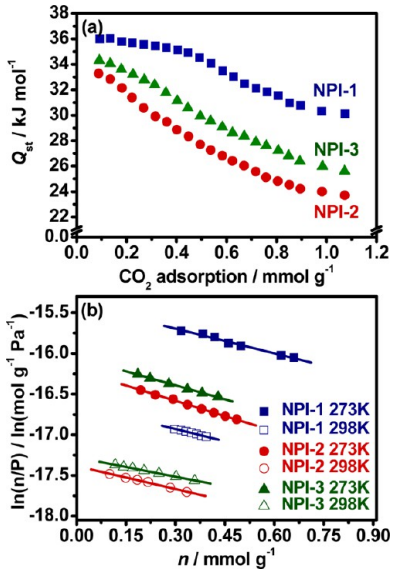

Figure 10. (a) Variation of CO_2 isosteric enthalpies with the adsorbed amount. (b) Virial plots of CO_2 adsorptions for NPI-1, NPI-2, and NPI-3.

Moreover, the Q_{st} values of NPI-1, NPI-2, and NPI-3 have the same ranking order as the surface areas, pore volumes, and CO_2 adsorption capacities. The above results suggest that, in addition to the affinity of CO_2 toward pore wall, the isosteric enthalpy of adsorption can also rely on the accessible ability of CO_2 molecule into the pores of the polymer. In this regard, the Q_{st} values can be influenced by the topological structure and the interconnectivity of the pore channels in the network to some extent.

More information about the interaction between CO_2 and pore wall of NPIs, such as Henry's law constants (K_H), the first virial coefficient (A_0), second virial coefficient (A_1), and enthalpy of adsorption at zero coverage (Q_0), can be obtained by analyzing the CO_2 isotherms at different temperatures using the virial equation[49]

$$\ln(n/P) = A_0 + A_1 n + A_2 n^2 + \ldots \quad (2)$$

where n is the adsorbed amount at pressure P and A_0, A_1, etc., are virial coefficients. At low surface coverage, A_2 and higher terms can be neglected, and there should be a linear relationship of $\ln(n/P)$ versus n. A_0 is related to the gas–material interaction, whereas A_1 reflects gas–gas interaction. The Henry's law constant (K_H) is calculated by equation of $K_H = \exp(A_0)$. Based on the K_H values at different temperature, the enthalpy of adsorption (Q_0) at zero surface CO_2 coverage is derived from the slope of the plot of $\ln K_H$ versus $1/T$.

Figure 10b shows that all the virial graphs of CO_2 at different temperatures give good straight lines, from which the values of A_0, A_1, K_H, and Q_0 were calculated, and the data are listed in Table 4. Similar to sorption capacities, it is observe that the A_0 and K_H values decrease with the increase of temperature since the adsorbate–adsorbent interaction becomes weaker, reflecting the physisorption characteristic of CO_2 on NPIs. The Q_0 values calculated for NPI-1, NPI-2, and NPI-3 are 33.5, 30.1, and 33.3 kJ mol^{-1}, respectively, which are higher than or comparable to other porous materials.[50−57]

In addition to the adsorption capacity, the ability of selective adsorption of CO_2 from other gases like N_2 and CH_4 is vitally important for the practical capture of CO_2 from the flue gas and purification of natural gas. For this purpose, the sorption isotherms of CH_4 and N_2 at 273 and 298 K were measured and are compared with those of CO_2. The curves in Figure 11 show that CO_2 has the considerably higher uptake than N_2 and CH_4 over the whole pressure range. The ratio of initial slope of CO_2 to N_2 is used as a measure of the selective adsorption of CO_2/N_2 gas pair (Table 3). For NPI-1, the separation factor of CO_2/N_2 is up to 88.6 at 273 K, which surpasses or is comparable to those for zeolitic imidazole frameworks (ZIFs, 20−50),[43] noncovalent porous materials (NPMs, 74),[58] and Bio-MOF-11 (81)[59] and comparable to benzimidazole-linked polymers (BILPs, 59−113).[51,52]

For the CO_2/N_2 gas pair to be separated, the enthalpy of adsorption of CO_2 is bigger than that of the inert gas N_2. As a result, relative to N_2, the decrease of adsorption capacity of CO_2 with temperature is more apparent. The data in Table 3 show that CO_2/N_2 selectivities of all the three samples have a decrease at 298 K compared to those at 273 K. However, it should be noted that, even though the temperature is increased to 298 K, NPI-1 still exhibits the high gas selectivity of CO_2/N_2 (45.2). This characteristic is very useful for the CO_2 adsorption/separation at room temperature.

The excellent selective adsorption of CO_2 for NPI-1 is attributed to the following four factors: (i) The high contents of oxygen and nitrogen atoms from the imide heterocycles in the NPI-1 network effectively enhance the affinity for CO_2 owing to the dipole–quadrupole interactions between the pore surface and CO_2 molecule,[60−62] leading to its high selective adsorption over other gases. (ii) As is well-known, the kinetic diameter is equal to the intermolecular distance of two molecules collision with zero initial kinetic energy and is taken as the smallest diameter that allows the gas molecule to enter the inner cavity, whereas the kinetic diameter of CO_2 (3.30 Å) is smaller than that of N_2 (3.64 Å).[63] In this regard, the high CO_2/N_2 selectivity is probably resulted from the narrow pore size distributions and ultrasmall pores (ca. 6.0 Å) in the NPI-1 network. (iii) The critical temperature of CO_2 gas is 304 K, much higher than that of N_2 (126 K).[64] The previous reports have demonstrated that the gas solubility coefficient in a polymer is positively correlated with its critical temperature.[65] As a result, compared to N_2 gas, CO_2 has the stronger

Table 4. K_H, A_0, A_1, and Q_0 Values of CO_2 Adsorption in the Microporous Polyimides

samples	T (K)	K_H (mol g^{-1} Pa^{-1})	A_0 (mol g^{-1} Pa^{-1})	A_1 (g mol^{-1})	Q_0 (kJ mol^{-1})
NPI-1	273	2.069×10^{-7}	−15.391	−1012.175	33.5
	298	6.012×10^{-8}	−16.627	−1009.352	
NPI-2	273	9.149×10^{-8}	−16.207	−1246.763	30.1
	298	3.018×10^{-8}	−17.316	−941.408	
NPI-3	273	1.074×10^{-7}	−16.047	−1147.650	33.3
	298	3.138×10^{-8}	−17.277	−749.655	

dx.doi.org/10.1021/jp408502t | J. Phys. Chem. C 2013, 117, 24428−24437

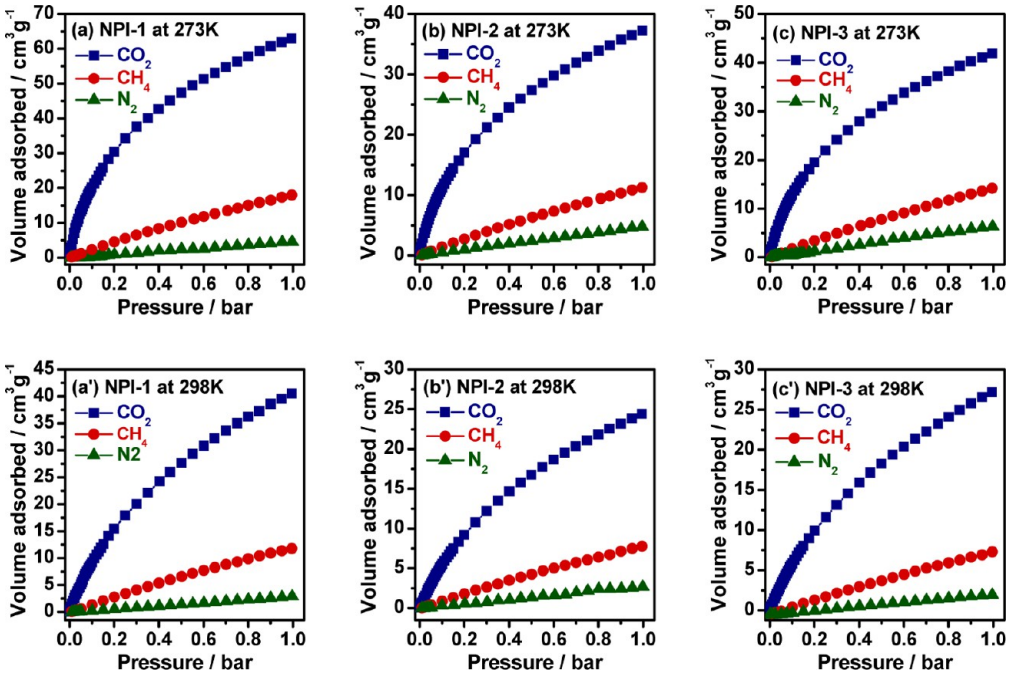

Figure 11. Adsorption isotherms of CO_2, CH_4, and N_2 gases at 273 K for NPI-1 (a), NPI-2 (b), and NPI-3 (c) and 298 K for NPI-1 (a′), NPI-2 (b′), and NPI-3 (c′).

adsorption ability with polymer skeleton, leading to the remarkably higher uptake of CO_2 than N_2. (iv) The tetrahedral building blocks in the NPI-1 network may play a significant role on the selective adsorption of CO_2 from N_2. Although the real reason is still unclear, the experimental results suggest that, compared to NPI-2 and NPI-3 constructed from triangular units, NPI-1 exhibits an apparently higher CO_2/N_2 separation factor.

On the other hand, the selective adsorptions of CO_2 over CH_4 are also evaluated. The data in Table 3 show that separation factors for NPI-1, NPI-2, and NPI-3 are 12.9, 12.3, and 11.1 at 273 K, respectively, which are comparable to other microporous polymers[51,52] and some of ZIFs.[43] Similar to the CO_2/N_2 gas pair, for all the three samples, the adsorption selectivities of CO_2 over CH_4 have a decrease with the increase of temperature. In addition, CH_4 has the higher critical temperature (191 K) than N_2 (126 K)[64] so that the affinity of CH_4 toward polymer skeleton is stronger than that of N_2. Therefore, in each case, the selective adsorption of CO_2/CH_4 is lower than that of CO_2/N_2.

CONCLUSIONS

In summary, three naphthalene-based microporous polyimide networks with uniform micropores were prepared by using naphthalene-1,4,5,8-tetracarboxylic dianhydride to polymerize with tetra(4-aminophenyl)methane, tris(4-aminophenyl)amine, and 1,3,5-tris(4-aminophenyl)benzene, respectively. Their chemical structures were well characterized by FTIR spectra, solid-state ^{13}C CP/MAS NMR spectra, and elemental analyses. The polymers are amorphous in nature and exhibit excellent thermal stability with the maximum weight loss over 550 °C. The BET surface areas of the three polymers vary in the range from 291 to 721 $m^2\ g^{-1}$, depending on the stereoconfiguration of the net nodes in the network. The results show that the naphthalene-based networks offer a strong affinity and selective adsorption toward benzene vapor. For example, the benzene vapor uptake is as high as 90.5 wt %, and its separation factors at 298 K for benzene/N_2, benzene/cyclohexane, and benzene/H_2O can reach 759.3, 13.8, and 40.3, respectively. In addition, the presence of large amounts of imide heterocycles in polymer skeletons endows polymers with high enthalpies of CO_2 adsorption (30.1−33.5 kJ mol^{-1}) and large adsorption capacity (12.3 wt %) at 1.0 bar and 273 K. The selectivities for CO_2/N_2 and CO_2/CH_4 are up to 88.6 and 12.9, respectively, superior to many other microporous organic polymers. The excellent adsorption/separation properties were investigated and discussed by the correlation with the porous structures of the networks as well as π-electrons, kinetic size, and critical temperatures of vapor or gas molecules and their affinity toward polymer skeletons.

ASSOCIATED CONTENT

Supporting Information

This section contains four figures and one table, including the WAXD curves, adsorption selectivities of CO_2 over CH_4 and N_2 at 273 and 298 K of the polyimide networks. This material is available free of charge via the Internet at http://pubs.acs.org.

AUTHOR INFORMATION

Corresponding Author

*E-mail: zgwang@dlut.edu.cn (Z.W.).

Notes

The authors declare no competing financial interest.

ACKNOWLEDGMENTS

We thank the National Science Foundation of China (Nos. 51073030 and 51273031) and the Program for New Century Excellent Talents in University of China (No. NCET-06-0280) for financial support of this research.

REFERENCES

(1) McKeown, N. B.; Budd, P. M. Polymers of Intrinsic Microporosity (PIMs): Organic Materials for Membrane Separations, Heterogeneous Catalysis and Hydrogen Storage. *Chem. Soc. Rev.* **2006**, *35*, 675−683.

(2) Dawson, R.; Cooper, A. I.; Adams, D. J. Nanoporous Organic Polymer Networks. *Prog. Polym. Sci.* **2012**, *37*, 530−563.

(3) Wu, D.; Xu, F.; Sun, B.; Fu, R.; He, H.; Matyjaszewski, K. Design and Preparation of Porous Polymers. *Chem. Rev.* **2012**, *112*, 3959−4015.

(4) Ding, S. Y.; Wang, W. Covalent Organic Frameworks (COFs): from Design to Applications. *Chem. Soc. Rev.* **2013**, *42*, 548−568.

(5) Zou, X.; Ren, H.; Zhu, G. Topology-Directed Design of Porous Organic Frameworks and Their Advanced Applications. *Chem. Commun.* **2013**, *49*, 3925−3936.

(6) Li, G. Y.; Wang, Z. G. Microporous Polyimides with Uniform Pores for Adsorption and Separation of CO_2 Gas and Organic Vapors. *Macromolecules* **2013**, *46*, 3058−3066.

(7) Luo, Y.; Li, B.; Wang, W.; Wu, K.; Tan, B. Hyper-Cross-Linked Aromatic Heterocyclic Microporous Polymers: A New Class of Highly Selective CO_2 Capturing Materials. *Adv. Mater.* **2012**, *46*, 3058−3066.

(8) Chen, Q.; Luo, M.; Hammershøj, P.; Zhou, D.; Han, Y.; Laursen, B. W.; Yan, C. G.; Han, B. H. Microporous Polycarbazole with High Specific Surface Area for Gas Storage and Separation. *J. Am. Chem. Soc.* **2012**, *134*, 6014−6087.

(9) Lu, W. G.; Yuan, D. Q.; Sculley, J.; Zhao, D.; Krishna, R.; Zhou, H. C. Sulfonate-Grafted Porous Polymer Networks for Preferential CO_2 Adsorption at Low Pressure. *J. Am. Chem. Soc.* **2011**, *133*, 18126−18129.

(10) Dawson, R.; Stöckel, E.; Holst, J. R.; Adams, D. J.; Cooper, A. I. Microporous Organic Polymers for Carbon Dioxide Capture. *Energy Environ. Sci.* **2011**, *4*, 4239−4245.

(11) Wang, Z. G.; Zhang, B. F.; Yu, H.; Sun, L. X.; Jiao, C. L.; Liu, W. S. Microporous Polyimide Networks with Large Surface Areas and Their Hydrogen Storage Properties. *Chem. Commun.* **2010**, *46*, 7730−7732.

(12) Preis, E.; Widling, C.; Brunklaus, G.; Schmidt, J.; Thomas, A.; Scherf, U. Microporous Polymer Networks (MPNs) Made in Metal-Free Regimes: Systematic Optimization of a Synthetic Protocol toward N-Arylcarbazole-Based MPNs. *ACS Macro Lett.* **2013**, *2*, 380−383.

(13) Ghanem, B. S.; Msayib, K. J.; McKeown, N. B.; Harris, K. D. M.; Pan, Z.; Budd, P. M.; Butler, A.; Selbie, J.; Book, D.; Walton, A. A Triptycene-Based Polymer of Intrinsic Microposity That Displays Enhanced Surface Area and Hydrogen Adsorption. *Chem. Commun.* **2007**, *43*, 67−69.

(14) Germain, J.; Svec, F.; Fréchet, J. M. J. Preparation of Size-Selective Nanoporous Polymer Networks of Aromatic Rings: Potential Adsorbents for Hydrogen Storage. *Chem. Mater.* **2008**, *20*, 7069−7076.

(15) Tan, D. Z.; Fan, W. J.; Xiong, W. N.; Sun, H. X.; Li, A.; Deng, W. Q.; Meng, C. G. Study on Adsorption Performance of Conjugated Microporous Polymers for Hydrogen and Organic Solvents: The Role of Pore Volume. *Eur. Polym. J.* **2012**, *48*, 705−711.

(16) Palkovits, R.; Antonietti, M.; Kuhn, P.; Thomas, A.; Schüth, F. Solid Catalysts for the Selective Low-Temperature Oxidation of Methane to Methanol. *Angew. Chem., Int. Ed.* **2009**, *48*, 6909−6912.

(17) Chen, L.; Yang, Y.; Jiang, D. L. CMPs as Scaffolds for Constructing Porous Catalytic Frameworks: A Built-in Heterogeneous Catalyst with High Activity and Selectivity Based on Nanoporous Metalloporphyrin Polymers. *J. Am. Chem. Soc.* **2010**, *132*, 9138−9143.

(18) Carta, M.; Malpass-Evans, R.; Croad, M.; Rogan, Y.; Jansen, J. C.; Bernardo, P.; Bazzarelli, F.; McKeown, N. B. An Efficient Polymer Molecular Sieve for Membrane Gas Separations. *Science* **2013**, *339*, 303−307.

(19) Qian, H.; Zheng, J.; Zhang, S. Preparation of Microporous Polyamide Networks for Carbon Dioxide Capture and Nanofiltration. *Polymer* **2013**, *54*, 557−564.

(20) Du, N.; Dal-Cin, M. M.; Robertson, G. P.; Guiver, M. D. Decarboxylation-Induced Cross-Linking of Polymers of Intrinsic Microporosity (PIMs) for Membrane Gas Separation. *Macromolecules* **2013**, *45*, 5134−5139.

(21) Zhang, B. F.; Wang, Z. G. Microporous Thermosetting Film Constructed from Hyperbranched Polyarylate Precursors Containing Rigid Tetrahedral Core: Synthesis, Characterization, and Properties. *Chem. Mater.* **2010**, *22*, 2780−2789.

(22) Rochelle, G. T. Amine Scrubbing for CO_2 Capture. *Science* **2009**, *325*, 1652−1654.

(23) Khan, F. I.; Ghoshal, A. K. Removal of Volatile Organic Compounds from Polluted Air. *J. Loss Prevent. Process Ind.* **2000**, *13*, 527−545.

(24) Ramos, M. E.; Bonelli, P. R.; Cukierman, A. L.; Ribeiro Carrott, M. M. L.; Carrott, P. J. M. Adsorption of Volatile Organic Compounds onto Activated Carbon Cloths Derived from A Novel Regenerated Cellulosic Precursor. *J. Hazard. Mater.* **2010**, *177*, 175−182.

(25) Shim, W. G.; Moon, H.; Lee, J. W. Performance Evaluation of Wash-Coated MCM-48 Monolith for Adsorption of Volatile Organic Compounds and Water Vapors. *Microporous Mesoporous Mater.* **2006**, *94*, 15−28.

(26) Shen, C. J.; Bao, Y. J.; Wang, Z. G. Tetraphenyladamantane-Based Microporous Polyimide for Adsorption of Carbon Dioxide, Hydrogen, Organic and Water Vapors. *Chem. Commun.* **2013**, *49*, 3321−3323.

(27) Wang, X. S.; Liu, J.; Bonefont, J. M.; Yuan, D. Q.; Thallapally, P. K.; Ma, S. Q. A Porous Covalent Porphyrin Framework with Exceptional Uptake Capacity of Saturated Hydrocarbons for Oil Spill Cleanup. *Chem. Commun.* **2013**, *49*, 1533−1535.

(28) Luo, J.; Xu, H.; Liu, Y.; Zhao, Y.; Daemen, L. L.; Brown, C.; Timofeeva, T. V.; Ma, S.; Zhou, H. C. Hydrogen Adsorption in A Highly Stable Porous Rare-Earth Metal-Organic Framework: Sorption Properties and Neutron Diffraction Studies. *J. Am. Chem. Soc.* **2008**, *130*, 9626−9627.

(29) Rzepka, M.; Lamp, P.; de la Casa-Lillo, M. A. Physisorption of Hydrogen on Microporous Carbon and Carbon Nanotubes. *J. Phys. Chem. B* **1998**, *102*, 10894−10898.

(30) Dou, B.; Li, J.; Hua, Q.; Ma, C.; He, C.; Li, P.; Hu, Q.; Hao, Z.; Qiao, S. Hydrophobic Micro/Mesoporous Silica Spheres Assembled from Zeolite Precursors in Acidic Media for Aromatics Adsorption. *Microporous Mesoporous Mater.* **2010**, *133*, 115−123.

(31) Farha, O. K.; Bae, Y. S.; Hauser, B. G.; Spokoyny, A. M.; Snurr, R. Q.; Mirkin, C. A.; Hupp, J. T. Chemical Reduction of A Diimide Based Porous Polymer for Selective Uptake of Carbon Dioxide Versus Methane. *Chem. Commun.* **2010**, *46*, 1056−1058.

(32) Wang, Z. G.; Zhang, B. F.; Yu, H.; Li, G. Y.; Bao, Y. J. Synthetic Control of Network Topology and Pore Structure in Microporous Polyimides Based on Triangular Triphenylbenzene and Triphenylamine Units. *Soft Matter* **2011**, *7*, 5723−5730.

(33) Yang, Y. Q.; Zhang, Q.; Zhang, Z. G.; Zhnag, S. B. Functional Microporous Polyimides Based on Sulfonated Binaphthalene Dianhydride for Uptake and Separation of Carbon Dioxide and Vapors. *J. Mater. Chem. A* **2013**, *1*, 10368−10374.

(34) Miller, R. D.; Burland, D. M.; Jurich, M.; Lee, V. Y.; Moylan, C. R.; Thackara, J. I.; Twieg, R. J.; Verbiest, T.; Volksen, W. Donor-Embedded Nonlinear-Optical Side-Chain Polyimides Containing No Flexible Tether-Materials of Exceptional Thermal-Stability for Electro-optic Applications. *Macromolecules* **1995**, *28*, 4970−4974.

(35) Yeh, R. M.; Xu, J.; Seeber, G.; Raymond, K. N. Large M4L4 (M = Al(III), Ga(III), In(III), Ti(IV)) Tetrahedral Coordination Cages: An Extension of Symmetry-Based Design. *Inorg. Chem.* **2005**, *44*, 6228−6239.

(36) Dawson, R.; Laybourn, A.; Clowes, R.; Khimyak, Y. Z.; Adams, D. J.; Cooper, A. I. Functionalized Conjugated Microporous Polymers. *Macromolecules* **2009**, *42*, 8809−8816.

(37) Weber, J.; Thomas, A. Toward Stable Interfaces in Conjugated Polymers: Microporous Poly(p-Phenylene) and Poly(Phenyleneethynylene) Based on a Spirobifluorene Building Block. *J. Am. Chem. Soc.* **2008**, *130*, 6334−6335.

(38) Lillo-Ródenas, M. A.; Cazorla-Amorós, D.; Linares-Solano, A. Benzene and Toluene Adsorption at Low Concentration on Activated Carbon Fibres. *Adsorption* **2011**, *17*, 473−481.
(39) Zhang, J. P.; Chen, X. M. Exceptional Framework Flexibility and Sorption Behavior of A Multifunctional Porous Cuprous Triazolate Framework. *J. Am. Chem. Soc.* **2008**, *130*, 6010−6017.
(40) Yu, H.; Shen, C. J.; Tian, M. Z.; Qu, J.; Wang, Z. G. Microporous Cyanate Resins: Synthesis, Porous Structure, and Correlations with Gas and Vapor Adsorptions. *Macromolecules* **2012**, *45*, 5140−5150.
(41) Yu, H.; Shen, C. J.; Wang, Z. G. Micro- and Mesoporous Polycyanurate Networks Based on Triangular Units. *ChemPlusChem* **2013**, *78*, 498−505.
(42) Rose, M.; Bohlmann, W.; Sabo, M.; Kaskel, S. Element−Organic Frameworks with High Permanent Porosity. *Chem. Commun.* **2008**, 2462−2464.
(43) Banerjee, R.; Furukawa, H.; Britt, D.; Knobler, C.; O'Keeffe, M.; Yaghi, O. M. Control of Pore Size and Functionality in Isoreticular Zeolitic Imidazolate Frameworks and their Carbon Dioxide Selective Capture Properties. *J. Am. Chem. .Soc.* **2009**, *131*, 3875−3877.
(44) An, J.; Geib, S. J.; Rosi, N. L. High and Selective CO_2 Uptake in a Cobalt Adeninate Metal-Organic Framework Exhibiting Pyrimidine- and Amino-Decorated Pores. *J. Am. Chem. Soc.* **2010**, *132*, 38−39.
(45) Furukawa, H.; Yaghi, O. M. Storage of Hydrogen, Methane, and Carbon Dioxide in Highly Porous Covalent Organic Frameworks for Clean Energy Applications. *J. Am. Chem. Soc.* **2009**, *131*, 8875−8883.
(46) Ren, S. J.; Dawson, R.; Laybourn, A.; Jiang, J. X.; Khimyak, Y.; Adams, D. J.; Cooper, A. I. Functional Conjugated Microporous Polymers: from 1,3,5-Benzene to 1,3,5-Triazine. *Polym. Chem.* **2012**, *3*, 928−934.
(47) Ben, T.; Pei, C. Y.; Zhang, D. L.; Xu, J.; Deng, F.; Jing, X. F.; Qiu, S. L. Gas Storage in Porous Aromatic Frameworks (PAFs). *Energy Environ. Sci.* **2011**, *4*, 3991−3999.
(48) Krungleviciute, V.; Heroux, L.; Migone, A. D. Isosteric Heat of Argon Adsorbed on Single-Walled Carbon Nanotubes Prepared by Laser Ablation. *J. Phys. Chem. B* **2005**, *109*, 9317−9320.
(49) Cole, J. H.; Everett, D. H.; Marshall, C. T.; Paniego, A. R.; Powl, J. C.; Rodriguez-Reinoso, F. Thermodynamics of High Temperature Adsorption of Some Permanent Gases by Porous Carbons. *J. Chem. Soc., Faraday Trans.* **1974**, *70*, 2154−2169.
(50) Martín, C. F.; Stöckel, E.; Clowes, R.; Adams, D. J.; Cooper, A. I.; Pis, J. J.; Rubiera, F.; Pevida, C. Hyper-Cross-Linked Organic Polymer Networks as Potential Adsorbents for Pre-Combustion CO_2 Capture. *J. Mater. Chem.* **2011**, *21*, 5475−5483.
(51) Rabbani, M. G.; El-Kaderi, H. M. Template-Free Synthesis of a Highly Porous Benzimidazole-Linked Polymer for CO_2 Capture and H_2 Storage. *Chem. Mater.* **2011**, *23*, 1650−1653.
(52) Rabbani, M. G.; Reich, T. E.; Kassab, R. M.; Jackson, K. T.; El-Kaderi, H. M. High CO_2 Uptake and Selectivity by Triptycene-Derived Benzimidazole-Linked Polymers. *Chem. Commun.* **2012**, *48*, 1141−1143.
(53) Yu, H.; Tian, M. Z.; Shen, C. J.; Wang, Z. G. Facile Preparation of Porous Polybenzimidazole Networks and Adsorption Behavior of CO_2 Gas, Organic and Water Vapors. *Polym. Chem.* **2013**, *4*, 961−968.
(54) Jackson, K. T.; Rabbani, M. G.; Reich, T. E.; El-Kaderi, H. M. Synthesis of Highly Porous Borazine-Linked Polymers and Their Application to H_2, CO_2, and CH_4 Storage. *Polym. Chem.* **2011**, *2*, 2775−2777.
(55) Reich, T. E.; Behera, S.; Jackson, K. T.; Jena, P.; El-Kaderi, H. M. Highly Selective CO_2/CH_4 Gas Uptake by a Halogen-Decorated Borazine-Linked Polymer. *J. Mater. Chem.* **2012**, *22*, 13524−13528.
(56) Demessence, A.; D'Alessandro, D. M.; Foo, M. L.; Long, J. R. Strong CO_2 Binding in a Water-Stable, Triazolate-Bridged Metal-Organic Framework Functionalized with Ethylenediamine. *J. Am. Chem. Soc.* **2009**, *131*, 8784−8786.
(57) Fu, Y. H.; Sun, D. R.; Chen, Y. J.; Huang, R. K.; Ding, Z. X.; Fu, X. Z.; Li, Z. H. An Amine-Functionalized Titanium Metal-Organic Framework Photocatalyst with Visible-Light-Induced Activity for CO_2 Reduction. *Angew. Chem., Int. Ed.* **2012**, *51*, 3364−3367.
(58) Lewinski, J.; Kaczorowski, Y.; Prochowicz, D.; Lipinska, T.; Justyniak, I.; Kaszkur, Z.; Lipkowski, J. Cinchona Alkaloid-Metal Complexes: Noncovalent Porous Materials with Unique Gas Separation Properties. *Angew. Chem., Int. Ed.* **2010**, *49*, 7035−7039.
(59) An, J. H.; Geib, S. J.; Rosi, N. L. High and Selective CO_2 Uptake in a Cobalt Adeninate Metal-Organic Framework Exhibiting Pyrimidine- and Amino-Decorated Pores. *J. Am. Chem. Soc.* **2010**, *132*, 38−39.
(60) Li, J. R.; Kuppler, R. J.; Zhou, H. C. Selective Gas Adsorption and Separation in Metal-Organic Frameworks. *Chem. Soc. Rev.* **2009**, *38*, 1477−1504.
(61) Panda, T.; Pachfule, P.; Chen, Y.; Jiang, J.; Banerjee, R. Amino Functionalized Zeolitic Tetrazolate Framework (ZTF) with High Capacity for Storage of Carbon Dioxide. *Chem. Commun.* **2011**, *47*, 2011−2013.
(62) Arstad, B.; Fjellvag, H.; Kongshaug, K. O.; Swang, O.; Blom, R. Amine Functionalised Metal Organic Frameworks (Mofs) as Adsorbents for Carbon Dioxide. *Adsorption* **2008**, *14*, 755−762.
(63) Breck, D. W. *Zeolite Molecular Sieves*; John Wiley & Sons: New York, 1994.
(64) Jeans, J. *An Introduction to the Kinetic Theory of Gases*; Cambridge University Press: London, 1982.
(65) Shah, V. M.; Hardy, B. J.; Stern, S. A. Solubility Of Carbon-Dioxide, Methane, and Propane in Silicone Polymers-Effect of Polymer Side-Chains. *J. Polym. Sci., Polym. Phys. Ed.* **1986**, *24*, 2033−2047.